Transactions on Machine Intelligence 2(3) (2019) 180-190

ISSN Online: 2821-1693

Transactions on Machine Intelligence

Journal Homepage: https://tmachineintelligence.ir/index.php/TMI

An Intelligent Method for Detecting and Classifying Dental Caries from Dental Radiographic Images

M. Kowsaryan[1], M. Taghizadeh[2,*], J. Jamali[3]

[1] Department of Electrical Engineering, Faculty of Engineering, Kazerun Branch, Islamic Azad University, Kazerun, Iran
[2] Department of Electrical Engineering, Faculty of Engineering, Kazerun Branch, Islamic Azad University, Kazerun, Iran
[3] Department of Electrical Engineering, Faculty of Engineering, Kazerun Branch, Islamic Azad University, Kazerun, Iran

ARTICLE INFO

Article History:
Received 17 May 2019
Received in revised form 22 June 2019
Accepted 13 September 2019
Available online 14 September 2019

Keywords:
X-Ray Images, Unsupervised Learning, Dental Caries

ABSTRACT

In recent years, dental image processing has become an essential tool in the early diagnosis and management of dental diseases, particularly dental caries. This technology addresses inherent limitations in traditional dental radiographs, such as low contrast and overlapping anatomical structures. However, despite technological progress, the accurate detection of dental caries remains a challenging task primarily due to the variability and non-uniformity of dental X-ray images. Most existing computer-aided diagnostic (CAD) systems rely heavily on supervised learning models that require large, annotated datasets. These models often perform sub optimally when confronted with images that differ significantly from the training data, leading to diagnostic inaccuracies. In this study, we propose an innovative method for tooth segmentation and caries detection from a diverse set of dental X-rays using an unsupervised learning approach. Unlike conventional systems, the proposed method employs a diagnostic protocol inspired by clinical dental evaluations, enabling the system to assess carious lesions relative to the structure and features of each individual image rather than relying on fixed detectors. Experimental results demonstrate that our method achieves a diagnostic accuracy of 96%, outperforming current supervised approaches. These findings highlight the robustness and adaptability of the proposed unsupervised framework, making it a promising solution for real-world dental diagnostic applications.

1. INTRODUCTION

Medical imaging is a crucial and evolving field in healthcare. Technological advancements in medical imaging represent a significant step toward effective healthcare. These advancements enhance early detection and accurate assessment of diseases, leading to timely patient treatment [1]. Pre-diagnostic analytical support provides a broader scope for physicians to treat patients more precisely. Dental caries is one of the most common diseases in modern societies, affecting approximately 36% of the global population [2]. Historically, developing countries were considered at lower risk of dental caries due to lower sugar consumption. For example, Africa had a 19% lower rate

* Corresponding Author: M.taghizadeh@kau.ac.ir
Department of Electrical Engineering, Faculty of Engineering, Kazerun Branch, Islamic Azad University, Kazerun, Iran

http://dx.doi.org/10.47176/TMI.2019.180

than the global average, while the Americas and European regions had rates 14% and 10% higher than the global average, respectively [3]. Despite this lower rate in the past, lifestyle changes have increased dental caries rates in African countries, worsening the situation. Early detection and treatment of dental caries, before the tooth root deteriorates, are essential for managing the disease. Digital radiography has been available in dentistry for over 30 years, with its use steadily increasing among dental professionals. In dental practice, post-processed digital radiographic images are widely used [4]. Computational image processing improves image quality and enhances diagnostic accuracy for dental radiographs. Processing techniques can effectively guide the diagnosis and assessment of dental diseases and damage [5]. Dental radiography displays the internal structure and organization of teeth via electromagnetic radiation. Dental X-ray images assist in identifying problems related to teeth, mouth, and jaw, including cavities, hidden dental structures (such as wisdom teeth), and bone loss that is not visible through visual examination. These radiographs are effective for detecting the early stages of tooth decay [6]. Four types of dental radiography exist [7]: Bitewing, Periapical, Occlusal, and Panoramic. Dental caries, caused by microorganisms affecting the hard tissues of teeth and found in the enamel surface, is classified into enamel caries, dentinal caries, and pulpal caries [8]. The initial diagnosis involves examining tooth surfaces with an appropriate optical system such as a dental mirror. Dental radiography provides a broader view of caries, especially interproximal caries, which are not visible through visual inspection. For superficial caries, visual examination by the dentist is sufficient, but radiographic imaging is necessary for detecting internal or interproximal caries. Accurate interpretation of dental radiographs requires significant expertise from the dentist. This paper proposes an image processing method for dental radiographs, utilizing computational intelligence and image processing techniques to diagnose and segment dental caries.

2. PRE-PROCESSING

To optimize the diagnostic effectiveness of the proposed method, it is essential to enhance the quality of X-ray images to be processed. This is achieved through image quality enhancement techniques, starting with noise removal and image improvement. Initially, the image is cleaned to remove any artifacts from the radiographic process that may affect the results. Techniques such as iterative and adaptive thresholding are applied to ensure that the images contain only pixels related to teeth, gums, and jawbone. Each image undergoes a cleansing filter to remove artifacts related to the positioning device, PID, which is defined later in this paper. Additionally, reference information embedded in the image by the dental X-ray software is removed, as it does not contribute to computer vision techniques.

3. IMAGE ENHANCEMENT

Once non-organic structures are removed, image contrast can be adjusted. To preserve feature details, noise removal through blur filters is avoided. Using noise removal techniques discussed in reference [9] and image enhancement methods in reference [10], a Median filter is applied first, followed by histogram equalization. The effects of this process can be observed in Figure 3-2.

3.1. Iterative Thresholding

Using the model proposed in reference [11] as a basis, iterative thresholding is employed to outline the general framework of teeth in the X-ray image. An intelligent edge detector is used, followed by morphological dilation to isolate pixels in the presumed dental boundary area. Approximately half of the obtained pixels belong to the teeth, while the other half corresponds to the jawbone and background objects. The initial threshold is computed from the average pixel values of presumed dental and background areas as follows:

$$\mu_D^i = \frac{\sum(i,j) \in dental\ f(i,j)}{\#dental\_pixels} \quad (1)$$

$$\mu_B^i = \frac{\sum(i,j) \in dental\ f(i,j)}{\#background\_pixels} \quad (2)$$

$$T_{i+1} = \frac{\mu_B^i + \mu_D^i}{2} \tag{3}$$

Where f(i,j) is the grayscale value of a pixel at (i,j), μDi and μBi are the average grayscale values for the dental and background areas, respectively, and T_{i+1} is the threshold for the entire image computed from the average pixel values of the background and teeth.

3.2. Adaptive Thresholding

Although iterative thresholding can be implemented without modifications, adaptive thresholding as described in reference [11] did not work well with the dataset used in this study. In standard adaptive thresholding, a pixel is thresholded if its grayscale value is less than the average of all non-zero pixels within an I*J window. The adaptive thresholding formula is:

$$T(i,j) = \frac{\sum_{s=-\frac{1}{2}}^{\frac{1}{2}} f(i+s,j+t)}{\#nozero\_pixels} \tag{4}$$

Even with histogram equalization performed before thresholding, some background pixels fell within the variance of dental pixels. Additionally, due to cavities, some dental pixels appeared darker than the background pixels, potentially affecting the diagnostic algorithm. Applying adaptive thresholding to masks from 40 images yields a threshold value. A global threshold is determined by averaging these thresholds. When each image is thresholded to obtain its specific threshold, the same process is applied. The final threshold is calculated from the weighted sum of these two values, with an initial weight of 0.5 for each threshold. If there is a difference of 10% or more between the two values, the following rule is applied:

$$FT(i,j) = \begin{cases} 0.6PAT + 0.4GAT, & if \quad 1 - \frac{PAT}{GAT} \geq 0.1 \\ 0.4PAT + 0.6GAT, & if \quad 1 - \frac{GAT}{PAT} \geq 0.1 \end{cases} \tag{5}$$

where FT is the final threshold, PAT is the personal adaptive threshold, and GAT is the global adaptive threshold.

4. TOOTH SEGMENTATION

For segmenting the mask obtained from the previous step, a whole-image approach is applied. This method is based on analyzing pixel intensity and detecting darker pixels within the image. When the whole-image method is applied to the masks, areas with zero-pixel values, removed in the previous step, are reintroduced. Since the system cannot distinguish whether the masks belong to the upper or lower jaw, all valleys are accepted at this stage, representing the cusps between the roots of some teeth. To determine the initial segmentation line, the center of each valley is used as a segmentation pixel to create dividing lines. These pixels are clustered to identify potential segmentation points within the image.

4.1. Boundary Detection and Enhancement

Before dental caries can be detected, it is essential to define the boundary of the tooth. At this stage, most non-dental pixels have been removed; however, the inability to perform a secondary pass of image transformation means that residual background components remain in regions where the tooth exhibits low contrast. To eliminate these residual components and prepare the image for boundary detection via active contour implementation, a binary filter is applied to each image. The threshold value for this binary filter is set such that when adjusted to a low intensity level, it yields optimal results, removing 80 to 90 percent of the remaining background elements. Consequently, a simple edge detector cannot be used effectively. Due to the effects of Top and Bottom Hat transformations, narrow teeth experience a series of disruptions in their contiguous pixels, attributed to the darker contrast of the tooth's core. It has been demonstrated that implementing active contours neutralizes this issue. Expanding the internal energy formula illustrates the components of elasticity and curve shape. By isolating the elasticity component of the formula

and extracting the α value, it becomes evident that setting an appropriate α value can constrain the elasticity of the curve. The following formula demonstrates how this component is obtained and how a sufficiently high α value neutralizes the effect of distance between points on the curve, thereby limiting the elasticity of the curve:

$$E_{internal} = \sum_{i=0}^{n-1} \alpha \|v_{i+1} - v_i\|^2 + \beta \|v_{i+1} - 2v_i + v_{i-1}\|^2 \quad (6)$$

$$E_{elastic} = \alpha \sum_{i=0}^{n-1} \left((x_{i+1} - x_i)^2 + (y_{i+1} - y_i)^2 - \bar{d}\right)^2 \quad (7)$$

where $v_i = (x_i, y_i)$ and d is the average distance between point pairs on the curve.

5. DETECTION OF DENTAL CARIES

The search space defined by the previous method delineates an area where dental caries are likely to be detected. Implementing a spot detector allows the identification of regions where dental caries may be present. Due to the high contrast in the image at this stage, resulting from the application of Top and Bottom Hat filters, carious lesions appear as significantly darker regions compared to the tooth material. This preferred spot detection algorithm has the capability to determine local maxima. To achieve a region of interest that remains unaffected by tooth scaling variations, a spot detection model as outlined in reference [12] is implemented. This model employs a Laplacian of Gaussian method to detect darker regions, defined by a convolution kernel as follows:

$$LoG = \frac{x^2+y^2-2\sigma^2}{\sigma^4} e^{-\frac{x^2+y^2}{2\sigma^2}} \quad (8)$$

where σ is the kernel width. The above relationship can be approximated by a 5x5 matrix as follows:

$$LoG = \begin{bmatrix} 0 & 0 & 1 & 0 & 0 \\ 0 & 1 & 2 & 1 & 0 \\ 1 & 2 & -16 & 2 & 1 \\ 0 & 1 & 2 & 1 & 0 \\ 0 & 0 & 1 & 0 & 0 \end{bmatrix} \quad (9)$$

Any region with sufficient contrast is revealed by the spot detector. Subsequently, darker pixels within these regions are clustered into distinct groups using a connectivity kernel described in Figure 1. Utilizing a four-way kernel results in the loss of some areas around the edges of the carious lesion clusters, negatively impacting the diagnostic method.

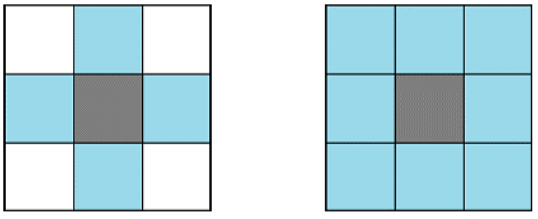

Fig.1. Two example kernels that can be used for connectivity clustering.

5.1. Analysis of Dental Caries

To determine if dental caries are manifesting using an unsupervised approach, standard dental analysis techniques need to be implemented. The search area was previously defined relative to the tooth, ranging from 10% to 15% of the tooth's total width. The average tooth size, as defined in reference [13], approximates tooth widths between 7.5 mm and 9 mm. Since the processed images are not panoramic X-rays, the exact tooth to be analyzed is not specified, as there is no way to predict tooth distribution. To estimate the tooth width, the following formula is used:

$$W = T_{max} - \frac{T_{variance}(P_{max} - P_{calculated})}{P_{variance}} \quad (10)$$

where W is the estimated width, T is the tooth width, and P is the percentage depth of the search space previously set between 10% and 15%. By calculating the maximum and minimum values for tooth width, $T_{variance}$ is determined to be 1.5. Similarly, $P_{variance}$ is computed as 5. This formula is based on the assumption that teeth requiring smaller analysis areas show a narrower range of tooth sizes, whereas teeth with wider search areas represent a broader range of sizes.

5.2. Cluster Analysis

To analyze whether a pixel cluster meets the criteria for dental caries classification, several acceptance factors are calculated. Initially, a threshold is computed based on the average pixel value of the cluster area. Then, a second threshold is computed based on the average intensity of pixels in the surrounding area. Since dental caries originate from enamel, the search space is ideally restricted to this region, as dentin appears darker in X-ray images. Enamel thickness varies between 0.87 mm and 1.45 mm, so an elliptical region is created with its center aligned perpendicular to the cluster, having a width equal to twice its height. The height is calculated using the following formula:

$$E = E_{max} - \frac{E_{variance}(T_{max} - T_{calculated})}{T_{variance}} \tag{11}$$

H represents the height of the ellipse, E denotes the enamel width, and T indicates the dentin width. By calculating the difference between the maximum and minimum values of enamel width, the $T_{variance}$ is found to be 0.58. This restricts the threshold mean production to only adjacent pixels within the enamel region. At this stage, to determine whether there is significant variance between these two regions, the two values are compared. If a cluster is less than 5% darker than the surrounding area, it is not considered, and no dental caries is detected. If the cluster area is more than 15% darker than the surrounding areas, the cluster is identified as a decayed region. If the cluster mean is between 5% and 15% darker, the algorithm proceeds to determine whether the cluster represents a shadow from the X-ray itself or an early stage of progressing dental caries. To detect significant gradient changes in this region, a Sobel operator with a 3×3 kernel is applied to the elliptical area. By limiting the kernel size to the minimum possible value, this operator can be applied to the region of interest of any size. To address the inherent inaccuracy of the 3×3 Sobel kernel, the Scharr function is used, which is defined by two kernels as follows:

$$G_x = \begin{bmatrix} -3 & 0 & +3 \\ -10 & 0 & +10 \\ -3 & 0 & +3 \end{bmatrix} \qquad G_y = \begin{bmatrix} -3 & 10 & -3 \\ 0 & 0 & 0 \\ +3 & +10 & +3 \end{bmatrix} \tag{12}$$

These kernels are applied to all pixels in the analyzed region, resulting in the transformation:

$$G = |G_x| + |G_y| \tag{13}$$

where G is the value of the new pixel. If no significant edge is detected using this algorithm, it implies that there is no significant change in pixel intensity within the search area. Therefore, the cluster is considered to be an X-ray shadow.

6. DATASET

The dataset used for testing consists of 115 periodontal X-ray images, with each image having 748 pixels in width and 512 pixels in height. The grayscale levels for each image range from [0,255]. The test images include a diverse selection of teeth such as molars, incisors, and wisdom teeth.

Fig.2. Examples of different X-ray scenarios present in the dataset: (a) X-ray showing adjacent wisdom teeth, (b) X-ray with a missing tooth, (c) X-ray where the contrast darkens across the image width.

In addition to the errors and artifacts described above, various conditions such as filled teeth, missing teeth, and adjacent teeth are commonly found in dental X-rays. Figure 2 shows some of these scenarios that are present in the test set. Table 1summarizes the composition of the dataset.

Table 1. Dataset

	Upper Jaw	**Lower Jaw**
Total number of images	37	78
Total number of teeth	141	239
Artifacts due to PID misalignment	3	20
Films underexposed to radiation	0	1
Films overexposed to radiation	3	0
The number of filled teeth	43	57

7. SIMULATION AND ANALYSIS

To process the dataset, a five-stage detection scheme is proposed as the best method for handling dental X-ray images. In the previous chapter, each stage is detailed separately. An overview of these five stages is as follows:

1. Preprocessing
2. Tooth Segmentation
3. Tooth Border Detection
4. Caries Feature Extraction
5. Caries Classification

7.1. Segmentation Results

The results regarding the effectiveness of the segmentation methods described in this paper are presented in two ways. The first method involves separating the performance metrics for the upper and lower jaws and evaluating each individually. This method provides insight into how well the algorithm performs on different jaw areas. The second method groups the two areas, thereby providing an average and overall success rate for the algorithm. For the purposes of this paper, the results are compared as separately as possible for each jaw area. Table 2 shows the results of the segmentation process. If the separation line does not cause partial separation of the teeth, the segmentation is considered to be correctly performed. Teeth previously partially segmented due to being on the edge of the X-ray are assumed to be fully segmented if they no longer cause partial segmentation.

Table 2. Segmentation Results

	Upper Jaw	Lower Jaw
Total number of teeth in 114 images	141	239
The number of correctly separated teeth	120	216
Correct percentage of teeth separation	85	90

Table 3. Comparison of Regional Segmentation Results

	Upper Jaw	Lower Jaw
Reference [29]	84%	81%
Proposed Method	85%	90%

Table 4. Comparison of Overall Segmentation Results

Implementation method	Accuracy (%)	Ref.
Thresholding	82.5	[29]
Thresholding	83	[52]
Active contour	58.1	[38]
Thresholding and full image	77.23	[28]
Active contour without edges	71.91	[16]
Area growth	83	[53]
Thresholding and full image	87.5	Present Study

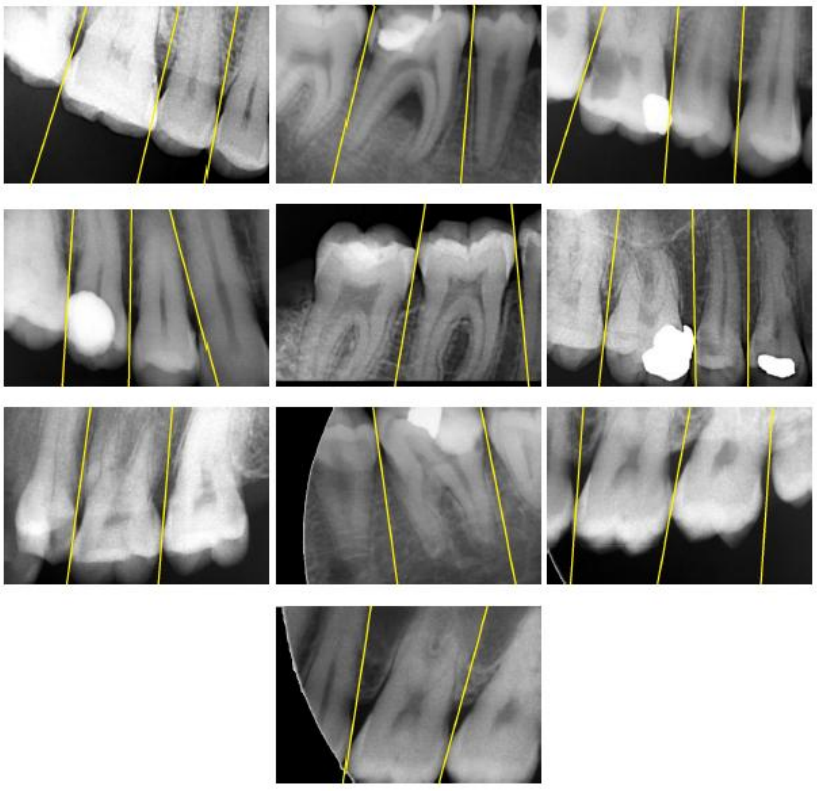

Fig.3. Examples of Segmentation Results from Test Dataset

Teeth with very poor contrast or those in close proximity were not segmented accurately. A regional comparison of these results with those from Reference [11] regarding the segmentation process is shown in Table 3. It should be

noted that combining previous algorithms with the new algorithm has improved segmentation results. Table 4 shows a comparison of the proposed method with segmentation processes implemented in various references. These results indicate that the proposed method in this paper has achieved a significant improvement over other method. Additionally, the diagnostic algorithm receives the highest number of accurately segmented images for evaluation. Figure 3 displays examples of the segmentation results.

7.2. Results of Caries Detection

To evaluate the success of the caries detection method, a reference dataset is utilized. This dataset includes markers for identified caries locations and also markers for false-positive regions. False-positive regions are defined as areas along the boundary of each tooth where caries was incorrectly identified, due to misinterpretation of the area, which may be due to X-ray contrast or because of a partial set of caries detectors leading the algorithm to interpret these areas as caries. Table 5 shows the success rate of the caries detection algorithm for identifying caries locations in the reference dataset, while Table 6 provides more detailed information on the identified caries regions. Figure 4 illustrates a scenario where the reference table only contains false-positive markers for teeth with actual caries. To determine if these rates fall within acceptable ranges, a comparison with various existing diagnostic methods is conducted, including caries detection performed by dentists using the Logicon caries detection system discussed in Reference [12]. The results of this comparison can be seen in Table 7.

Table 5. Caries Detection Results

	Upper Jaw	**Lower Jaw**
The total number of decays in the reference table	28	41
The number of correctly identified teeth	26	29
Percentage of correct identification (%)	93	91

Table 6. Detailed Results of Caries Detection

	Upper Jaw	**Lower Jaw**
The number of correctly classified teeth	136	220
Number of false positives	3	7
The number of missing decays	2	12
Percentage of correct classification of teeth	96	92
The percentage of false positives	2	3
Percentage of missing caries	3	5

b **a**

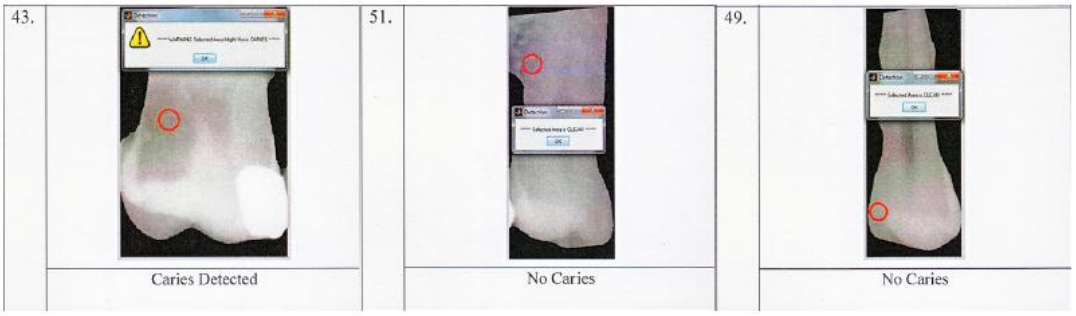

c

Fig. 4. Examples of Results Obtained by the Caries Detection Algorithm and Comparison with Reference Table; (a) original image, (b) Segmented image with identified caries, (c) Reference table data

Table 7. Comparison of Caries Detection Results

Percentage of missing caries	Percentage of false positives	Percentage of correct classifications	Ref.
6	-	94	[14]
20	20	60	[15]
2	-	98	[16]
10	-	90	[17]
2	2	96	Present Study

8. CONCLUSION

The diagnosis of dental caries through the implementation of an unsupervised model addresses the issues encountered with existing computer-aided diagnostic systems. This problem arises from the reliance of current diagnostic models on a database to make determinations about the data. Consequently, these systems become dependent on their training datasets and must confront scenarios that fulfill specific conditions, often leading to diagnostic errors such as false positives. Utilizing image analysis methods to determine the presence of dental caries helps create a system that emulates human diagnostic methods, allowing for caries detection based on visual interpretation of the teeth. This paper proposes an unsupervised learning model for detecting dental caries, which is implemented using a segmentation method to separate X-ray images into individual teeth, a boundary detection method to identify tooth edges for caries analysis, and a diagnostic algorithm that evaluates tooth boundaries using image processing techniques. The results from implementing this model indicate that the proposed method can detect up to 90% of dental caries.

Transparency Statement

The data supporting this study are available upon reasonable request to the corresponding author, subject to ethical and confidentiality considerations.

Acknowledgments

We would like to express our gratitude to all individuals who contributed to this project.

Declaration of Interest

The authors declare that they have no competing interests.

Funding

This research received no specific grant from any funding agency, commercial, or not-for-profit sectors.

REFERENCES

[1] Zabir, I., Paul, S., Rayhan, M. A., & Sarker, T. (2015). Automatic brain tumor detection and segmentation from multi-modal MRI images based on region growing and level set evolution. IEEE Transactions, 22(8), 241-255. https://doi.org/10.1109/WIECON-ECE.2015.7443979

[2] Vos, T., Flaxman, A. D., Naghavi, M., Lozano, R., Michaud, C., Ezzati, M., Shibuya, K., Salomon, J. A., Abdalla, S., Aboyans, V., et al. (2013). Years lived with disability (ylds) for 1160 sequelae of 289 diseases and injuries 1990-2010: A systematic analysis for the global burden of disease study 2010. The Lancet, 380(9859), 2163-2196.

[3] Moreira, R. S. (2012). Epidemiology of dental caries in the world. INTECH Open Access Publisher. https://doi.org/10.5772/31951

[4] Sakamoto, T. (2018). Medical image processing apparatus, medical image processing method, and medical image processing system. US Patent App, 31(2), 120-145.

[5] Boughattas, N., Berar, M., & Hamrouni, K. (2018). Feature selection and classification using multiple kernel learning for brain tumor segmentation. IEEE Transactions on Medical Imaging, 27(5), 1-5. https://doi.org/10.1109/ATSIP.2018.8364470

[6] Yao, J. (2016). Image processing in tumor imaging. In New Techniques in Oncologic Imaging (pp. 79-102).

[7] Rad, A. E., Amin, I. B. M., Rahim, M. S. M., & Kolivand, H. (2019). Computer-aided dental caries detection system from X-ray images. In S. Phon-Amnuaisuk & T. Au (Eds.), Computational Intelligence in Information Systems (pp. 233-243). Cham: Springer. https://doi.org/10.1007/978-3-319-13153-5_23

[8] Oliveira, J., & Proenca, H. (2019). Caries detection in panoramic dental X-ray images. In Computational Vision and Medical Image Processing (pp. 175-190). Netherlands: Springer. https://doi.org/10.1007/978-94-007-0011-6_10

[9] Yoon, J. H., & Ro, Y. M. (2002). Enhancement of the contrast in mammographic images using the homomorphic filter method. IEICE Transactions on Information and Systems, 85(1), 298-303.

[10] Ahmad, S. A., Taib, M. N., Khalid, N. E. A., & Taib, H. (2012). An analysis of image enhancement techniques for dental X-ray image interpretation. International Journal of Machine Learning and Computing, 2(3), 292-297. https://doi.org/10.7763/IJMLC.2012.V2.133

[11] Nomir, O., & Abdel-Mottaleb, M. (2005). A system for human identification from X-ray dental radiographs. Pattern Recognition, 38(8), 1295-1305. https://doi.org/10.1016/j.patcog.2004.12.010

[12] Veena Divya, K. V., Jatti, A., Joshi, R., & Krishna, S. D. (2017). Characterization of dental pathologies using digital panoramic X-ray images based on texture analysis. In Conference of the IEEE Engineering in Medicine and Biology Society (EMBC) (pp. 592-5). https://doi.org/10.1109/EMBC.2017.8036894

[13] Azerooni, A., Ahmadian, A., Saberi, H., Alirezaie, J., & Rad, H. (2012). An efficient algorithm for registration of pre- and intra-operative brain MRI images to correct intensity inhomogeneity. Information Science, Signal Processing and their Applications International Conference, 26(6), 8-253.

[14] Tracy, K. D., Dykstra, B. A., Gakenheimer, D. C., Scheetz, J. P., Lacina, S., Scarfe, W. C., & Farman, A. G. (2010). Utility and effectiveness of computer-aided diagnosis of dental caries. General Dentistry, 59(2), 136-144.

[15] Dykstra, B. (2008). Interproximal caries detection: How good are we? Dentistry Today, 27(4), 144-146.

[16] Oliveira, J. (2009). Caries detection in panoramic dental X-ray images. In Computational Vision and Medical Image Processing (pp. 251-270). Netherlands: Springer. https://doi.org/10.1007/978-94-007-0011-6_10

[17] Oliveira, J., & Proenca, H. (2019). Caries detection in panoramic dental X-ray images. In Computational Vision and Medical Image Processing (pp. 175-190). Netherlands: Springer. https://doi.org/10.1007/978-94-007-0011-6_10